J|A|C|S ARTICLES

Published on Web 04/22/2009

Magnetic Resonance Imaging Studies on Catalyst Impregnation Processes: Discriminating Metal Ion Complexes within Millimeter-Sized γ-Al_2O_3 Catalyst Bodies

Leticia Espinosa-Alonso,[†] Anna A. Lysova,[‡,§] Peter de Peinder,[†,⊥] Krijn P. de Jong,[†] Igor V. Koptyug,[‡] and Bert M. Weckhuysen*,[†]

Inorganic Chemistry and Catalysis group, Department of Chemistry, Faculty of Science, Utrecht University, Sorbonnelaan 16, 3508 TB Utrecht, The Netherlands, International Tomography Center SB RAS, Institutskaya Street 3A, Novosibirsk 630090, Russia, Boreskov Institute of Catalysis SB RAS, Pr. ac. Lavrentieva 5, Novosibirsk 630090, Russia, and VibSpec, Haaftenlaan 28, 4006 XL Tiel, The Netherlands

Received January 16, 2009; E-mail: b.m.weckhuysen@uu.nl

Abstract: Magnetic resonance imaging (MRI) was used to study the impregnation step during the preparation of Ni/γ-Al_2O_3 hydrogenation catalysts with Ni^{2+} metal ion present in different coordinations. The precursor complexes were $[Ni(H_2O)_6]^{2+}$ and $[Ni(edtaH_x)]^{(2-x)-}$ (where $x = 0$, 1, 2 and *edta* = ethylenediaminetetraacetic acid), representing a nonshielded and a shielded paramagnetic complex, respectively. Due to this shielding effect of the ligands, the dynamics of $[Ni(H_2O)_6]^{2+}$ or $[Ni(edtaH_x)]^{(2-x)-}$ were visualized applying T_2 or T_1 image contrast, respectively. MRI was applied in a quantitative manner to calculate the $[Ni(H_2O)_6]^{2+}$ concentration distribution after impregnation when it was present alone in the impregnation solution, or together with the $[Ni(edtaH_x)]^{(2-x)-}$ species. Moreover, the combination of MRI with UV−vis microspectroscopy allowed the visualization of both species with complementary information on the dynamics and adsorption/desorption phenomena within γ-Al_2O_3 catalyst bodies. These phenomena yielded nonuniform Ni distributions after impregnation, which are interesting for certain industrial applications.

1. Introduction

In order to gain insight into the physicochemical processes which take place during the preparation of supported catalyst bodies (with sizes from tens of micrometers to millimeters), spectroscopic techniques with space and time resolution are increasingly being developed and applied. Until recently, the spectroscopic techniques used to characterize catalyst bodies required a pretreatment of the sample under study, which generally consisted of bisecting the catalyst body, sometimes followed by a polishing treatment.[1−9] This pretreatment might influence the system, namely by polluting it. Therefore, the development of new characterization techniques which do not require the pretreatment of the catalyst material is advantageous. Of particular interest is the development of noninvasive techniques which allow to study the samples *in situ*; i.e. during the different preparation steps.[10,11] Magnetic resonance imaging (MRI) serves as an example of such noninvasive techniques. MRI is a technique commonly used in the field of medicine. The contrast or brightness in an NMR (nuclear magnetic resonance) image is a direct measure of the NMR signal intensity of water protons. This signal intensity can be made to depend on the proton nuclear spin relaxation times.[12−15] In medical applications, pathologic tissue and normal tissue can be distinguished because they have different proton relaxation times. Moreover, the contrast of an NMR image can be enhanced by the use of contrast agents, which decrease the relaxation times of protons. In medicine, paramagnetic gadolinium (III) complexes are widely used for this purpose, while other paramagnetic transition metal ions, such as nickel (II), copper (II) and cobalt (II), are also relevant to the design of paramagnetic

[†] Utrecht University.
[‡] International Tomography Center SB RAS.
[§] Boreskov Institute of Catalysis SB RAS.
[⊥] VibSpec.

(1) Bergwerff, J. A.; Jansen, M.; Leliveld, B. G.; Visser, T.; de Jong, K. P.; Weckhuysen, B. M. *J. Catal.* **2006**, *243*, 292.
(2) Bergwerff, J. A.; van de Water, L. G. A.; Visser, T.; de Peinder, P.; Leliveld, B. R. G.; de Jong, K. P.; Weckhuysen, B. M. *Chem.−Eur. J.* **2005**, *11*, 4592.
(3) Bergwerff, J. A.; Visser, T.; Leliveld, B. R. G.; Rossenaar, B. D.; de Jong, K. P.; Weckhuysen, B. M. *J. Am. Chem. Soc.* **2004**, *126*, 14548.
(4) Chen, H.-C.; Anderson, R. B. *Ind. Eng. Chem. Prod. Res. Dev.* **1973**, *12*, 122.
(5) Chen, H.-C.; Gillies, G. C.; Anderson, R. B. *J. Catal.* **1980**, *62*, 367.
(6) Espinosa-Alonso, L.; de Jong, K. P.; Weckhuysen, B. M. *J. Phys. Chem. C* **2008**, *112*, 7201.
(7) Kresge, C. T.; Chester, A. W.; Oleck, S. M. *Appl. Catal., A* **1992**, *81*, 215.
(8) van de Water, L. G. A.; Bergwerff, J. A.; Nijhuis, T. A.; de Jong, K. P.; Weckhuysen, B. M. *J. Am. Chem. Soc.* **2005**, *127*, 5024.
(9) van de Water, L. G. A.; Bezemer, G. L.; Bergwerff, J. A.; Versluijs-Helder, M.; Weckhuysen, B. M.; de Jong, K. P. *J. Catal.* **2006**, *242*, 287.
(10) Beale, A. M.; Jacques, S. D. M.; Bergwerff, J. A.; Barnes, P.; Weckhuysen, B. M. *Angew. Chem., Int. Ed.* **2007**, *46*, 8832.
(11) Bergwerff, J. A.; Lysova, A. A.; Espinosa Alonso, L.; Koptyug, I. V.; Weckhuysen, B. M. *Angew. Chem., Int. Ed.* **2007**, *46*, 7224.
(12) Bryar, T. R.; Daughney, C. J.; Knight, R. J. *J. Magn. Reson.* **2000**, *142*, 74.
(13) Kuhn, W. *Angew. Chem., Int. Ed.* **1990**, *29*, 1.
(14) Lauffer, R. B. *Chem. Rev.* **1987**, *87*, 901.
(15) Tomer, G.; Mantle, M. D.; Gladden, L. F.; Newton, J. M. *Int. J. Pharm.* **1999**, *189*, 19.

diagnostic agents.[14,16] Some of these metal ions are the active components in a large number of heterogeneous catalysts, making the MRI technique interesting in the field of catalyst preparation.[11,17−21] With the aid of MRI, the distribution and transport of complexes of paramagnetic transition metal ions inside a catalyst body upon their impregnation can be deduced by monitoring the ^{1}H NMR signal of the water solvent inside the catalyst body.[11,18,20]

Nitrate salts of paramagnetic transition metal ions are often used as precursors in the preparation of heterogeneous catalysts due to their attractive properties, such as high solubility, which enable the preparation of catalysts with high metal loadings in a single impregnation step. Important problems encountered in the preparation of catalysts, such as Ni/γ-Al_2O_3 hydrogenation catalysts, are the formation of metal aluminates and/or poor metal dispersion.[22−24] A way of avoiding the migration of metal ions into the bulk structure of alumina is the addition of complexing agents to the impregnation solution. Consequently, the molecular structure of the precursor complexes as well as the interactions of these complexes with the support is modified. Several studies on catalyst preparation have proven that the use of metal ion precursor solutions containing chelating ligands increases the metal oxide reducibility and dispersion.[25−31]

In this paper, the ^{1}H MRI-based method reported earlier[11] was applied to monitor and quantify the transport of $[Ni(H_2O)_6]^{2+}$ in γ-Al_2O_3 catalyst bodies. This investigation illustrates the general validity of this method. Moreover, MRI was also used to follow the transport of other Ni^{2+} complexes, viz. $[Ni(edtaH_x)]^{(2-x)-}$ ($x = 0, 1, 2$ *edta* = ethylenediaminetetraacetic acid). The bulky *edta* ligand shielded the paramagnetic effect of Ni^{2+} on the ^{1}H NMR signal and in this case a different experimental protocol was required to visualize Ni^{2+}. The combination of MRI with UV−vis microspectroscopy enabled us to discriminate $[Ni(H_2O)_6]^{2+}$ from $[Ni(edtaH_x)]^{(2-x)-}$ when both complexes were present in the impregnation solution, and $[Ni(H_2O)_6]^{2+}$ transport could be monitored in the presence of $[Ni(edtaH_x)]^{(2-x)-}$.

Table 1. Composition of the Ni-*edta* Impregnation Solutions and Speciation of the Ni^{2+} Complexes (as Determined from UV−Vis Spectroscopy, Supporting Information)

solution	[Ni] (M)	[*edta*] (M)	calcd concns of the species present[a]
Ni*edta*1:1pH1	0.1	0.1	0.05 M $[Ni(edtaH)]^-$ 0.05 M $[Ni(edtaH_2)]$
Ni*edta*1:1pH7	0.1	0.1	0.1 M $[Ni(edta)]^{2-}$
Ni*edta*6:1pH1	0.6	0.1	0.50 M $[Ni(H_2O)_6]^{2+}$ 0.07 M $[Ni(edtaH)]^-$ 0.03 M $[Ni(edtaH_2)]$
Ni*edta*6:1pH6	0.6	0.1	0.49 M $[Ni(H_2O)_6]^{2+}$ 0.11 M $[Ni(edta)]^{2-}$

[a] The protons in $[Ni(edtaH_x)]^{(2-x)-}$ ($x = 1, 2$) are forming carboxyl groups.[32,33]

2. Experimental Section

2.1. Preparation of the Impregnation Solutions. To quantify the dynamics of $[Ni(H_2O)_6]^{2+}$ inside a catalyst body after its impregnation, several $[Ni(H_2O)_6]^{2+}$ solutions were prepared with concentrations ranging from 0.1 to 1.0 M by dissolving the required amounts of $Ni(NO_3)_2 \cdot 6H_2O$ (Acros, p.a.) in deionized water.

Ni-*edta* solutions in a 1:1 molar ratio were prepared with 0.1 M $Ni(NO_3)_2 \cdot 6H_2O$ (Acros, p.a.) and 0.1 M *edta* precursor (*edta* = ethyelenediaminetetraacetic acid, Acros, p.a.) at pH 1 and 7. *Edta*-disodium precursor salt was used to achieve pH 1, and *edta*-tetrasodium precursor salt was used to obtain pH 7. These Ni-*edta* solutions will be referred to as Ni*edta*1:1pH1 and Ni*edta*1:1pH7. Two other Ni-*edta* solutions with a molar ratio Ni^{2+}:*edta* = 6:1 were prepared by slowly adding *edta*-disodium salt or *edta*-tetrasodium salt to an aqueous solution of $Ni(NO_3)_2 \cdot 6H_2O$. The final pH of these solutions were 1 (solution Ni*edta*6:1pH1) and 6 (solution Ni*edta*6:1pH6), respectively. The latter solution was not stable with time and a fresh solution was prepared for each experiment. Table 1 summarizes the composition and speciation of the Ni-*edta* solutions. The speciation of the Ni-*edta* complexes in solution, as a function of pH, was determined by using multivariate curve resolution analysis (MCR) of UV−vis spectra of the solutions. Information on the procedure followed to determine the speciation can be found in the Supporting Information.

UV−vis spectra of the impregnation solutions were recorded between 450 and 850 nm with a Cary 50 UV−vis spectrophotometer (Varian). Diffuse-reflectance UV−vis spectra of impregnated catalyst bodies were acquired between 250 and 1050 nm with the use of a home-built setup described elsewhere.[8] All UV−vis measurements of the impregnated catalyst bodies were performed along a scan-line through the resulting surface of the extrudates after bisection with a scalpel. Twelve spectra were collected along the diameter of the bisected extrudates. The spatial resolution was 320 μm and 5 min were required to collect the spectra along the scan-line.

2.2. Catalyst Preparation. γ-Al_2O_3 extrudates (12 mm long and 3.85 mm in diameter) with a BET surface area of 145 $m^2 \cdot g^{-1}$ and a pore volume of 0.36 $mL \cdot g^{-1}$, as determined from N_2-physisorption, were used. The point of zero charge (pzc) of the γ-Al_2O_3 extrudates was 7.9, as determined by mass titration.[34] Pore volume impregnation of single γ-Al_2O_3 extrudates was done dropwise along the extrudate, making sure that the entire extrudate was wetted. The volume added for impregnation of a single extrudate was equal to the pore volume plus 10%. Thus, the average volume used for a single extrudate was 90−100 μL, depending on the weight of the extrudate. This volume was added in drops of approximately 30 μL. After adding all the drops, the vial with the extrudate was shaken for 30 s and the remaining liquid (10% of the volume added) was removed with a pipet. The volume inside the extrudate was,

(16) Barnhart, J. L. P.; Berk, R. N. M. *Invest. Radiol.* **1986**, *21*, 132.
(17) Anderson, J. A.; Fernández Garcia, M. *Supported Metals in Catalysis*; Imperial College Press: London, 2005.
(18) Bergwerff, J. A.; Lysova, A. A.; Espinosa-Alonso, L.; Koptyug, I. V.; Weckhuysen, B. M. *Chem.−Eur. J.* **2008**, *14*, 2363.
(19) Ertl, G.; Knozinger, H.; Weitkamp, J. *Preparation of Solid Catalysts*; Wiley-VHC: Weinheim, 1999.
(20) Lysova, A. A.; Koptyug, I. V.; Sagdeev, R. Z.; Parmon, V. N.; Bergwerff, J. A.; Weckhuysen, B. M. *J. Am. Chem. Soc.* **2005**, *127*, 11916.
(21) Regalbuto, J. R. *Catalyst Preparation: Science and Engineering*; CRC Press: Boca Raton, 2007.
(22) Salagre, P.; Fierro, J. L. G.; Medina, F.; Sueiras, J. E. *J. Mol. Catal. A: Chem.* **1996**, *106*, 125.
(23) Sietsma, J. R. A.; Meeldijk, J. D.; den Breejen, J. P.; Versluijs-Helder, M.; van Dillen, A. J.; de Jongh, P. E.; de Jong, K. P. *Angew. Chem., Int. Ed.* **2007**, *46*, 4547.
(24) Sietsma, J. R. A.; Meeldijk, J. D.; Versluijs-Helder, M.; Broersma, A.; van Dillen, A. J.; de Jongh, P. E.; de Jong, K. P. *Chem. Mater.* **2008**, *20*, 2921.
(25) Molina, R.; Centeno, M. A.; Poncelet, G. *J. Phys. Chem. B* **1999**, *103*, 6036.
(26) Negrier, F.; Marceau, E.; Che, M.; Giraudon, J. M.; Gengembre, L.; Lofberg, A. *J. Phys. Chem. B* **2005**, *109*, 2836.
(27) Pasieczna-Patkowska, S.; Ryczkowski, J. *Appl. Surf. Sci.* **2007**, *253*, 5910.
(28) Ryczkowski, J. *React. Kinet. Catal. Lett.* **1989**, *40*, 189.
(29) Schimpf, S.; Louis, C.; Claus, P. *Appl. Catal., A* **2007**, *318*, 45.
(30) Sun, K.-Q.; Marceau, E.; Che, M. *Phys. Chem. Chem. Phys.* **2006**, *8*, 1731.
(31) van Dillen, A. J.; Terörde, R. J. A. M.; Lensveld, D. J.; Geus, J. W.; de Jong, K. P. *J. Catal.* **2003**, *216*, 257.
(32) Grant, M. W.; Dodgen, H. W.; Hunt, J. P. *J. Am. Chem. Soc.* **1971**, *93*, 6828.
(33) Smith, G. S.; Hoard, J. L. *J. Am. Chem. Soc.* **1959**, *81*, 556.
(34) Park, J.; Regalbuto, J. R. *J. Colloid Interface Sci.* **1995**, *175*, 239.

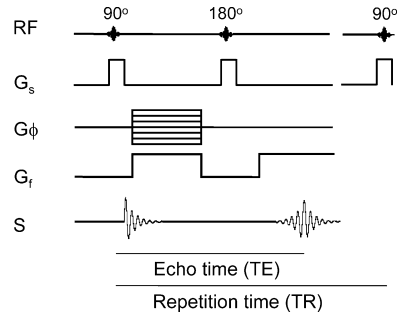

Figure 1. Timing diagram of a two-pulse spin−echo sequence. The echo time and the repetition time are also indicated. S indicates when the signal appears in the sequence.

Table 2. Summary of the Experimental Parameters Used for Detection of NMR Images and of the Type of Image Contrast Obtained

solution	[Ni] (M)	[Ni]:[*edta*]	TR (ms)	TE (ms)	contrast
$[Ni(H_2O)_6]^{2+}$	0.1−1.0	0	1000	1	T_2
Ni*edta*1:1	0.1	1	100	1	T_1
Ni*edta*6:1	0.6	6	1000	1	T_2

therefore, equal to the pore volume of the support. This means that the average concentration of Ni^{2+} inside the extrudate was constant during each MRI experiment and directly determined by the Ni^{2+} concentration of the impregnation solution.

2.3. MRI Experiments. Immediately after pore volume impregnation, the extrudates were placed inside an NMR tube. A wet tissue was inserted in the NMR tube to avoid drying of the extrudates during the measurements.

The NMR/MRI experiments were performed using a Bruker Avance DRX 300 (300 MHz) wide-bore spectrometer equipped with imaging accessories. The acquisition of two-dimensional (2D) cross-sectional images was based on the detection of the ^1H NMR signal of water in the impregnated extrudates with a two-pulse spin−echo sequence shown schematically in Figure 1. Two radiofrequency (RF) pulses with 90° and 180° flip angles were applied during the sequence. G_f and G_ϕ refer to the magnetic field gradients applied in the x direction (G_f, frequency encoding) and in the y direction (G_ϕ, phase encoding). In the z direction, slice selection was applied (G_s), and the signal recorded corresponded to a 2-mm slice in the center of the extrudates detected transverse to the sample axis. The echo time (TE) and repetition time (TR) are also shown in the figure. A detailed description on the fundamentals of MRI can be found elsewhere.[13,35,36]

Images were collected imposing either T_1 contrast or T_2 contrast. The echo time was fixed at TE = 1 ms. To obtain T_1-weighted images (T_1 contrast), TR was set to 100 ms. This value is in between the T_1 values of the two aqueous components in the sample (pure water and water in the presence of the Ni^{2+} complex). To obtain T_2-weighted images (T_2 contrast), the TR was 1 s, which was longer than the T_1 values of the two components. Table 2 summarizes the experimental parameters, TR and TE, and the contrast obtained in all the MRI experiments. Acquisition time of an image was 4.5 min (TR = 1 s) or 30 s (TR = 100 ms) and the spatial resolution in the image plane was 140 μm by 230 μm.

2.4. NMR Relaxation Time Experiments. Relaxation time measurements for all Ni^{2+} solutions saturating the pores of alumina extrudates were performed to determine the spin−lattice (T_1) and the spin−spin (T_2) relaxation times of water protons in the presence of Ni^{2+}. Inversion−recovery experiments were carried out to measure T_1 and Carr−Purcell−Meiboom−Gill (CPMG) experiments were performed to measure T_2.[35] The relaxation times relevant to the following discussion are summarized in Table 3.

Table 3. Relaxation Times T_1 and T_2 of Water in the Pores of Alumina Extrudates in the Presence of Different Ni^{2+} Complexes, and Magnetization Values[a]

solution	T_1 (ms)	T_2 (ms)	M_{T1}^{1s}	M_{T1}^{100ms}	M_{T2}	I/I_o^{1s}	I/I_o^{100ms}
H_2O	216.9	3.86	0.99	0.37	0.77	0.76	0.28
Ni*edta*1:1pH7	15.98	2.67	1.00	1.00	0.69	0.69	0.69
$[Ni(H_2O)_6]^{2+}$ 0.1 M	11.05	2.11	1.00	1.00	0.62	0.62	0.62

[a] $I/I_o = M_{T1} \times M_{T2}$, where $M_{T1} = [1 - \exp(-TR/T_1)]$ and $M_{T2} = [\exp(-TE/T_2)]$.

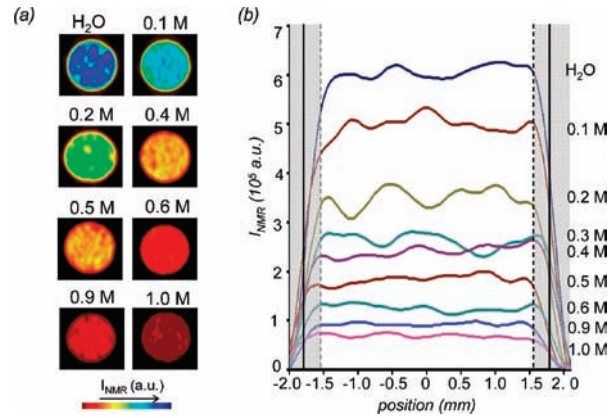

Figure 2. (a) T_2-weighted images of the extrudates 12 h after impregnation with aqueous Ni^{2+} solutions containing different concentrations of $[Ni(H_2O)_6]^{2+}$. (b) 1D signal intensity profiles in arbitrary units (au), as a function of the position inside the extrudates for different $[Ni(H_2O)_6]^{2+}$ concentrations. The gray areas indicate the regions excluded from quantitative data analysis.

3. Results and Discussion

3.1. Dynamics of $[Ni(H_2O)_6]^{2+}$ within γ-Al_2O_3 Catalyst Bodies Based on T_2 Contrast. Figure 2a shows the T_2-weighted images of extrudates impregnated with aqueous solutions with various Ni^{2+} concentrations after equilibration for 12 h. An image of an extrudate impregnated with water is also shown. In all cases, the images show a spatially uniform NMR signal and, therefore, a uniform macro-distribution of $[Ni(H_2O)_6]^{2+}$ in the extrudates. The relaxation of water protons is progressively enhanced with increasing concentration of paramagnetic species. In other words, a low NMR signal intensity corresponds to a high Ni^{2+} concentration (red color), whereas a high NMR signal intensity indicates a low Ni^{2+} concentration (blue color). This is because an increase in T_2 times corresponds to an increase in the NMR signal intensity (see expression for M_{T2} in the footnote of Table 3).

One-dimensional (1D) ^1H NMR signal intensity profiles (in arbitrary units, au), along a scan-line of the catalyst body, are shown in Figure 2b. The edges of the extrudates are marked as thick black vertical lines in the figure. The NMR signal in the edges does not show an abrupt signal change from a maximum value (inside the extrudates) to zero (outside the extrudates). This is due to the limited spatial resolution and smoothing of the NMR images for a better presentation. Consequently, extrudates boundaries appear smooth, with a gradual signal variation at the extrudates edges. This gradual signal variation corresponds to the gray regions in the figure. Moreover, smoothing of the inner extrudates regions does not lead to signal variations as the signal intensity is independent of position in

(35) Callaghan, P. T. *Principles of Nuclear Magnetic Resonance Microscopy*; Clarendon Press: Oxford, 1991.
(36) Lalith Talagala, S.; Lowe, I. J. *Concepts Magn. Reson.* **1991**, *3*, 145.

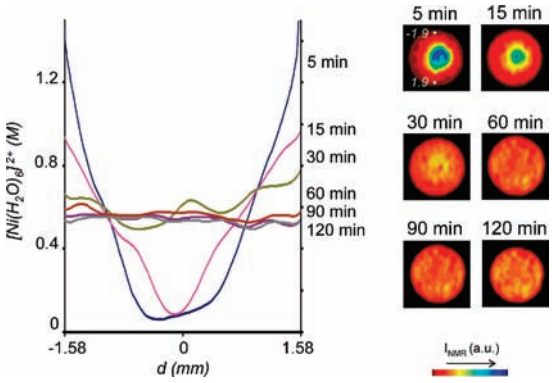

Figure 3. 1D profiles of the $[Ni(H_2O)_6]^{2+}$ concentration as a function of the position inside the extrudates at certain times after impregnation, together with the recorded T_2-weighted images.

the inner regions, but helps to average out noise and sample heterogeneities. Due to smoothing, the boundaries of the extrudates represented in gray color are excluded from data analysis, and only the data points from position −1.58 mm to 1.58 mm will be considered for data analysis, and depicted in the subsequent 1D profiles in Figures 3−7 (NMR signal profiles or concentration profiles).

The 1D signal intensity profiles show how the ^{1}H NMR signal decreases with increasing Ni^{2+} concentration. These profiles are not totally flat due to noise in the experimental measurements and the heterogeneities in alumina structure.[37] To have an idea of the uncertainty of the measurements, an additional experiment was performed. In this experiment, four different extrudates were impregnated with water and the measured 1D signal intensity profiles were averaged. The resulting relative standard deviation was calculated to be 4%. This value was taken as a basis for the measurement error.

The average NMR signal intensity along a scan-line of the Ni^{2+}-impregnated extrudates versus the Ni^{2+} concentration in the impregnation solution yielded the following exponential dependence ($R = 0.99$):

$$I_{NMR} = 50270 + 569106[\exp(-[Ni^{2+}]/0.332)] \qquad (1)$$

The fitted curve and a detailed description of the physical meaning of this exponential dependence can be found in the Supporting Information.

Figure 3 illustrates the 1D $[Ni(H_2O)_6]^{2+}$ concentration profile inside an extrudate as a function of time after pore volume impregnation. The impregnation solution contained 0.5 M $Ni(NO_3)_2$. The T_2-weighted images of the extrudate after impregnation with this solution are also depicted in this figure. The red regions indicate high Ni^{2+} concentrations and the blue regions correspond to low Ni^{2+} concentrations. The concentration profiles were obtained after applying the calibration curve, eq 1, to the 1D signal intensity profiles measured. At the edges of the extrudate, 5 min after impregnation, the $[Ni(H_2O)_6]^{2+}$ concentration was higher than 0.5 M, while in the center there was no nickel present. During the pore volume impregnation, three main phenomena occur: capillary flow of the solution toward the core of the extrudate, diffusion of the metal ion in the pores filled with water, and its adsorption on the walls of the pores.[38,39] The fact that $[Ni(H_2O)_6]^{2+}$ ions do not move toward the core of the catalyst body together with the capillary flow of water molecules, and that a concentration gradient is observed 5 min after impregnation, suggests that there are interactions of this complex with the pore walls of the alumina extrudate. Moreover, these interactions cannot be electrostatic since the slightly acidic pH of the $[Ni(H_2O)_6]^{2+}$ solution below the pzc of γ-Al_2O_3 creates a positively charged alumina surface. These interactions are responsible for the $[Ni(H_2O)_6]^{2+}$ concentration gradient, and, therefore, the transport of $[Ni(H_2O)_6]^{2+}$ toward the core takes place according to liquid phase diffusion and adsorption/desorption phenomena on the pore walls. A uniform distribution of 0.53 M $[Ni(H_2O)_6]^{2+}$ was achieved 60 min after impregnation, which agreed with the concentration of the impregnation solution. This calculated concentration was within the range of the expected uncertainty (4−10%, see Supporting Information). Moreover, the time needed to get a uniform distribution of $[Ni(H_2O)_6]^{2+}$ was in line with liquid phase diffusion of $Ni(NO_3)_2$ salt in bulk solution for a distance of 1.93 mm (radius of the γ-Al_2O_3 extrudate) which indicates that the adsorption of $[Ni(H_2O)_6]^{2+}$ on alumina surface is limited.[39,40]

Recently, an MRI study was performed on the quantification of $[Co(H_2O)_6]^{2+}$ transport after impregnation of similar γ-Al_2O_3 extrudates.[11] The range of concentrations that could be calibrated for $[Co(H_2O)_6]^{2+}$ was limited to a maximum value of 0.5 M, while $[Ni(H_2O)_6]^{2+}$ was calibrated up to 0.9 M, with 10% uncertainty. This difference is due to the paramagnetic properties of the two ions, with $[Co(H_2O)_6]^{2+}$ having a stronger paramagnetic effect on water protons and enhancing their relaxation rate to a larger extent than $[Ni(H_2O)_6]^{2+}$.

3.2. Dynamics of $[Ni(edtaH_x)]^{(2-x)-}$ within γ-Al_2O_3 Catalyst Bodies Based on T_1 Contrast. While a shorter T_2 time leads to a lower NMR signal intensity in T_2-weighted images, a shorter T_1 time leads to higher signal intensity in T_1-weighted images (see expressions for M_{T2} and M_{T1}, respectively, in the footnote of Table 3). Table 3 shows the T_1 and T_2 relaxation times of water protons inside a catalyst body impregnated with 0.1 M $[Ni(H_2O)_6]^{2+}$ or with 0.1 M $[Ni(edta)]^{2-}$ (solution Ni*edta*1: 1pH7). The relaxation times of pure water in a catalyst body are also presented as a reference. The relaxation times decreased in the presence of Ni^{2+} ions in all cases. Yet, when Ni^{2+} was present as $[Ni(edta)]^{2-}$, the relaxation times were longer than when Ni^{2+} was totally coordinated to water molecules. The spin−lattice and spin−spin relaxation rates (T_i^{-1}, $i = 1, 2$) of water protons are affected by various interactions between the paramagnetic complex and the solvent molecules. Usually, the relaxation rate is described as the sum of the contributions due to inner-sphere interactions and outer-sphere interactions between the metal ion and water molecules. It has been shown previously that the latter may have an important contribution to the total relaxation rate in the particular case of metal ion complexes with a low water coordination number.[14,41] *Edta* is a bulky ligand and the number of coordinated water molecules when Ni^{2+} is complexed to *edta* depends on the solution pH; at pH 7 the number of coordinated water molecules is essentially zero, and at pH 1 is 1, see Supporting Information. In these cases, *edta* impedes the strong paramagnetic effect of Ni^{2+} on water protons and the main contribution to the relaxation rates

(37) Koptyug, I. V.; Lysova, A. A.; Sagdeev, R. Z.; Parmon, V. N. *Catal. Today* **2007**, *126*, 37.
(38) Assaf, E. M.; Jesus, L. C.; Assaf, J. M. *Chem. Eng. J.* **2003**, *94*, 93.
(39) Neimark, A. V.; Kheifets, L. I.; Fenelonov, V. B. *Ind. Eng. Chem. Prod. Res. Dev.* **1981**, *20*, 439.
(40) Takahashi, R.; Sato, S.; Sodesawa, T.; Kamomae, Y. *Phys. Chem. Chem. Phys.* **2000**, *2*, 1199.
(41) Oakes, J.; Smith, E. G. *J. Chem. Soc., Faraday Trans.* **1983**, *79*, 543.

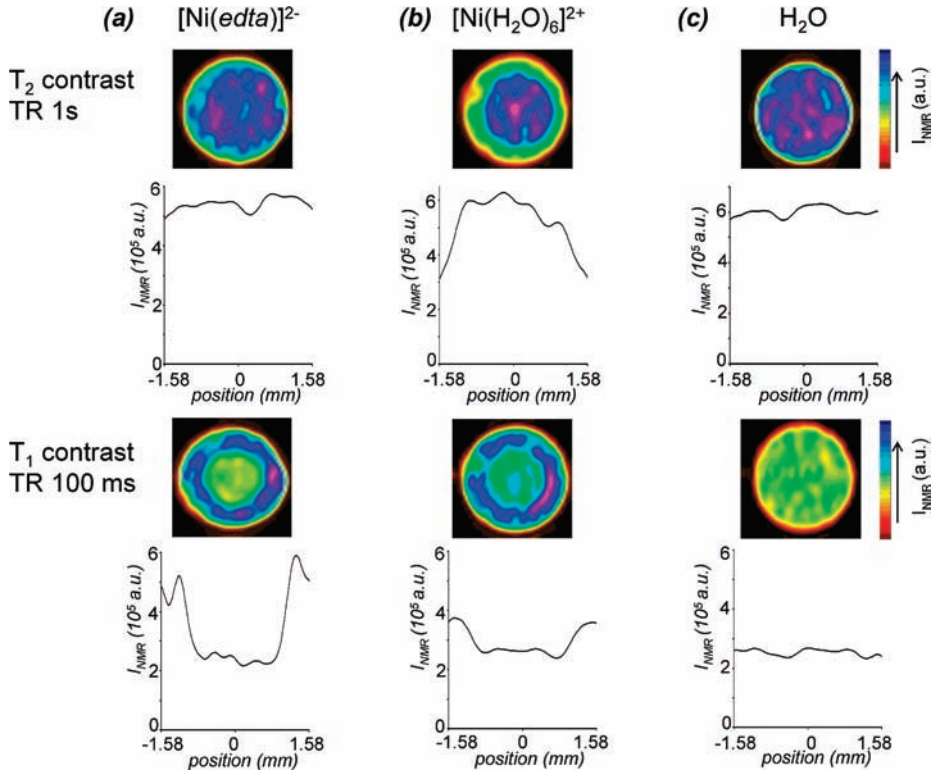

Figure 4. Images of catalyst bodies 5 min after impregnation with the solutions containing the complexes $[Ni(edta)]^{2-}$ (0.1 M) (a), $[Ni(H_2O)_6]^{2+}$ (0.1 M) (b) and pure water (c). The images were recorded with TR = 1 s (top) and TR = 100 ms (bottom). The 1D signal intensity profiles as a function of the position inside the catalyst bodies are also shown.

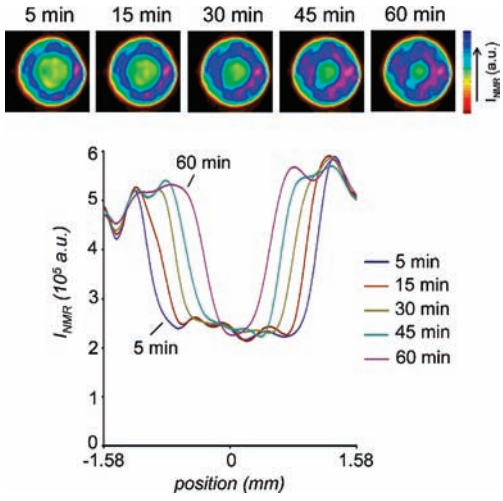

Figure 5. T_1-weighted images after impregnation of an extrudate with solution Ni*edta*1:1pH7, and the corresponding 1D signal intensity profiles as a function of the position inside the catalyst body.

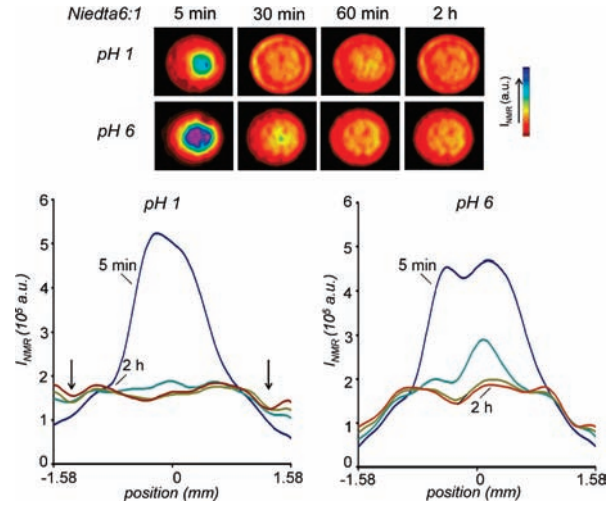

Figure 6. T_2-weighted images at several times after impregnation of extrudates with solutions Ni*edta*6:1pH1 and Ni*edta*6:1pH6, and the corresponding 1D signal intensity profiles as a function of the position inside the catalyst body.

is due to outer-sphere interactions with water. Conversely, in the case of $[Ni(H_2O)_6]^{2+}$, the relaxation of protons is caused by both inner-sphere and outer-sphere interactions with the water molecules; thus, the relaxation rates are faster.

Figure 4 shows the images and the corresponding 1D signal intensity profiles of extrudates impregnated with pure water and with 0.1 M $[Ni(H_2O)_6]^{2+}$ or 0.1 M Ni*edta*1:1pH7 solutions 5 min after impregnation. Two sets of images were collected with TR = 100 ms or 1 s. When the repetition time was 1 s (Figure 4 top), the T_2-weighted image of an extrudate containing water showed a uniform NMR signal intensity around 6×10^5 au. The NMR image of an extrudate containing 0.1 M $[Ni(H_2O)_6]^{2+}$ showed T_2 contrast, with an outer green ring indicating the presence of Ni^{2+} (lower NMR signal intensity) and the blue core representing the presence of pure water (NMR signal $\sim 6 \times 10^5$ au). With these working conditions (TR 1 s), the NMR signal is low where Ni^{2+} is present since the relaxation rate T_2^{-1} of water protons in the presence of Ni^{2+} is very fast (relaxation time T_2 is short, see Table 3); i.e., when the NMR signal is collected, the protons in the presence of Ni^{2+} have relaxed, giving a small NMR signal, see Table 3 (I/I_o^{1s}). The NMR image and the corresponding 1D signal intensity profile of an extrudate containing solution Ni*edta*1:1pH7 were almost

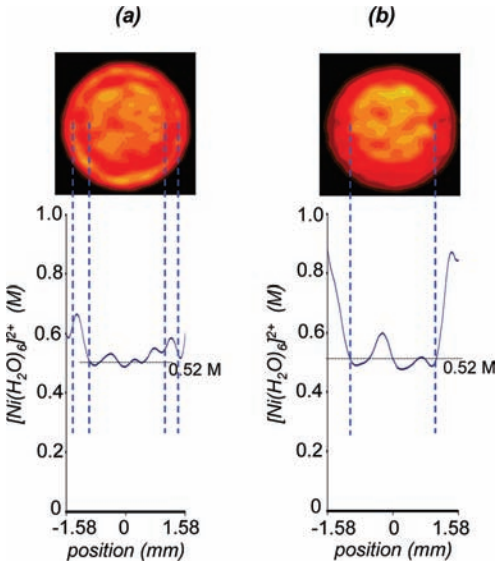

Figure 7. T_2-weighted images of extrudates 2 h after impregnation with solutions Ni*edta*6:1pH1 (a) and Ni*edta*6:1pH6 (b), and the corresponding $[Ni(H_2O)_6]^{2+}$ concentration profiles as a function of the position inside the extrudate constructed under the assumption that eq 1 is valid when Ni-*edta* complexes are present along with $[Ni(H_2O)_6]^{2+}$.

identical to those of pure water; thus, under these experimental conditions the NMR signal of water protons was insensitive to the presence of $[Ni(edta)]^{2-}$, and the transport of Ni^{2+} could not be visualized. In other words, the NMR signals of water in the presence and in the absence of $[Ni(edta)]^{2-}$ were too close to be distinguished from each other. For the repetition time of 100 ms (T_1-weighted images at the bottom of Figure 4), the NMR image of a water-impregnated extrudate showed a uniform color, and the corresponding 1D signal intensity profile indicated an average signal of 2×10^5 au. The NMR image of an extrudate containing $[Ni(H_2O)_6]^{2+}$ showed a mixed T_1-T_2 contrast, with a dominating contribution of T_1 contrast. The signal was the lowest in the core of the extrudate (green core), where pure water was present and its signal was suppressed (T_1 contrast). On the other hand, in the edges the NMR signal is low (blue ring) compared to that of pure water in the T_2-weighted image (see Figure 4c top) but is higher than in the core. Thus, both T_1 and T_2 affect the signal intensity profile (mixed T_1-T_2 contrast). The NMR image of the extrudate impregnated with solution Ni*edta*1:1pH7 exhibited pure T_1 contrast. The core of the extrudate, with an NMR signal of 2×10^5 au and a green color, indicated the presence of pure water. The outer ring in blue color was assigned to the presence of $[Ni(edta)]^{2-}$, as expected. At these working conditions (TR = 100 ms), water protons which are not in contact with Ni^{2+} complexes have long T_1 relaxation rates (longer than TR). This means that these protons do not have enough time to relax and their NMR signal is suppressed. In the edges, the NMR signal intensity is high due to the presence of Ni^{2+} complexes. The T_1 relaxation time of water protons decreases in the presence of Ni^{2+} complexes, and water protons have enough time to relax, giving a high NMR signal. The images were measured 5 min after impregnation, and Ni^{2+} had not yet reached the core of the extrudate, in any case.

Table 3 summarizes all these NMR signal intensity profiles in numbers. The NMR signal intensity of the 1D profiles measured is represented as I (or I/I_o) in eq 2:

$$I_{NMR}=I_o[1 - \exp(-TR/T_1)][\exp(-TE/T_2)] \quad (2)$$

If the known values of T_1, T_2, TR, and TE are substituted in eq 2, the quantities I/I_o^{1s} and I/I_o^{100ms} are obtained. The large TR values in comparison to the T_1 values in the presence of $[Ni(H_2O)_6]^{2+}$ or Ni*edta*1:1pH7 solutions are responsible for the absence of any influence of the spin−lattice relaxation on the total NMR signal ($M_{T1}^{100ms} \sim M_{T1}^{1s} \sim 1$ for these cases). On the other hand, a decrease in TR when the extrudates contain pure water induces a decrease in the NMR signal intensity ($M_{T1}^{100ms} = 0.37$).

In short, in order to visualize the transport of a shielded paramagnetic metal ion complex (e.g., $[Ni(edta)]^{2-}$), T_1 contrast should be created by choosing an adequate repetition time in the two-pulse spin−echo sequence. However, T_1 contrast can also be used to monitor the transport of a nonshielded metal ion complex ($[Ni(H_2O)_6]^{2+}$). Measuring T_1 contrast provides an increase in time resolution, which is advantageous if the transport of the metal ion under study is very fast. In this study, the use of TR = 100 ms decreases the acquisition time of one NMR image by a factor of 10.

Figure 5 shows the T_1-weighted images collected on an extrudate at several points in time after its impregnation with solution Ni*edta*1:1pH7 (complex $[Ni(edta)]^{2-}$). The blue external ring represents high NMR signal intensity values, and as explained above, it corresponds to the region where $[Ni(edta)]^{2-}$ is present. The green core indicates the presence of pure water (low NMR signal intensity). One hour after impregnation $[Ni(edta)]^{2-}$ still showed an egg-shell distribution inside the extrudate (blue external ring). It took 90 to 120 min (images not shown) to get a uniform distribution of this complex. This time was expected according to a liquid phase diffusion transport of $[Ni(edta)]^{2-}$ when limited interactions between the complex and the support's surface take place. Namely, it is assumed that $[Ni(edta)]^{2-}$ has a smaller diffusion coefficient than $[Ni(H_2O)_6]^{2+}$ since it is a bulkier complex. Moreover, electrostatic interactions between the complex and alumina surface are not very strong when the solution pH is close to the pzc of the support. The 1D signal intensity profiles as a function of the position inside the extrudate are also presented. Close to the edges, the NMR signal intensity remains constant with time after impregnation, since at these working conditions (TR = 100 ms) relaxation of water protons in the presence of $[Ni(edta)]^{2-}$ is fast enough. On the other hand, in the core, where no $[Ni(edta)]^{2-}$ is present after 5 min, water protons do not have time to relax, and their signal is suppressed. As $[Ni(edta)]^{2-}$ diffuses to the core, water protons in that region relax faster and ultimately have enough time to relax, recovering the maximum signal. Since these 1D profiles show NMR signal intensities and not concentrations, no conservation of the area under the curves of Figure 5 is expected.

The transport of Ni^{2+} was also monitored after impregnating a catalyst body with solution Ni*edta*1:1pH1. It has to be mentioned that alumina is not stable at very low pH values, and it can dissolve, forming $[Al(H_2O)_6]^{3+}$. An MRI experiment on a similar extrudate after its impregnation with an aqueous solution of 0.1 M HCl showed the same T_2-weighted image or 1D NMR signal intensity profile as if it were impregnated with water. Moreover, the stability of $[Ni(edtaH_x)]^{(2-x)-}$ ($x = 1, 2$) in the catalyst body was proven with UV−vis microspectroscopy, see Supporting Information. Therefore, dissolved Al^{3+} ions did not interact with Ni^{2+} to form other types of structures. This suggests that even though the possible dissolution of alumina cannot be excluded, it does not influence the NMR signal of

the water protons. The Ni*edta*1:1pH1 solution contained the complexes $[Ni(edtaH)]^-$ and $[Ni(edtaH_2)]$, see Table 1. It was not possible to distinguish the effect of one or the other complex on the ^1H NMR signal of water protons, and they were treated as a whole. At pH 1, Ni^{2+} was penta- or tetra-coordinated to *edta*, and to one or two water molecules. Yet, Ni^{2+} did not show a strong paramagnetic effect on the relaxation of proton nuclei, and its transport could not be visualized using T_2 contrast under our experimental conditions. T_1-weighted images collected during the dynamics of Ni^{2+} redistribution after impregnation of a catalyst body with this solution indicated a slower transport of $[Ni(edtaH_x)]^{(2-x)-}$ ($x = 1, 2$) compared to that of $[Ni(edta)]^{2-}$ (solution at pH 7), meaning that at pH 1 the adsorption of Ni^{2+} complexes on alumina surface was stronger. This was also observed, at pH 3, by Bowers et al.[42] At pH 1, alumina net surface charge was positive, facilitating the electrostatic interactions with negatively charged $[Ni(edtaH)]^-$ species. Moreover, the transport of $[Ni(edtaH_2)]$ toward the core induced the deprotonation of this species (due to an increase of the solution pH inside the pores) and the protonation of alumina surface. This acid−base equilibrium between $[Ni(edtaH_2)]$ and the alumina surface provoked the formation of $[Ni(edtaH)]^-$ and $[Ni(edta)]^{2-}$ which, at the same time, also adsorbed electrostatically on the surface of alumina.

3.3. Dynamics of $[Ni(H_2O)_6]^{2+}$ and $[Ni(edtaH_x)]^{(2-x)-}$ within γ-Al_2O_3 Catalyst Bodies Based on T_2 Contrast. As can be inferred from the previous section, when T_2 contrast (TR = 1 s) is applied to an extrudate impregnated with a solution containing both $[Ni(edtaH_x)]^{(2-x)-}$ and $[Ni(H_2O)_6]^{2+}$ (solutions Ni*edta*6:1pH1 or Ni*edta*6:1pH6), only the $[Ni(H_2O)_6]^{2+}$ complex should be visualized, see the top parts of (a) and (b) of Figure 4. This is true if there are no interactions between the two complexes or, in other words, if they behave independently inside the catalyst body. Assuming that this is the case and only the complex $[Ni(H_2O)_6]^{2+}$ is visualized, the diffusion of this complex can be deduced from the NMR images and the 1D NMR signal intensity profiles shown in Figure 6.

Figure 6 (top) shows the T_2-weighted images of two catalyst bodies after impregnation with solutions Ni*edta*6:1pH1 and Ni*edta*6:1pH6. The images measured 5 min after impregnation indicated a dark-red outer rim with a low NMR signal (strong paramagnetic influence and high $[Ni(H_2O)_6]^{2+}$ concentration) and a blue core with a high NMR signal (weak paramagnetic influence and low $[Ni(H_2O)_6]^{2+}$ concentration) in both cases. After 2 h, the images showed an internal ring with a dark-red color for the Ni*edta*6:1pH1 impregnated extrudate or an outer ring with a dark-red color for the Ni*edta*6:1pH6 impregnated extrudate. These images suggested an egg-white and an egg-shell Ni^{2+} macro-distribution, respectively. According to the reasoning presented at the beginning of this section, these egg-white and egg-shell distributions should reflect the distribution of $[Ni(H_2O)_6]^{2+}$, whereas no influence of the complex $[Ni(edtaH_x)]^{(2-x)-}$ on the ^1H NMR signal is expected.

Similarly, the 1D signal intensity profiles (Figure 6, bottom) pointed out a decrease in $[Ni(H_2O)_6]^{2+}$ concentration at the edges of the extrudate with time after impregnation (indicated by an increase of the NMR signal) and an increase in $[Ni(H_2O)_6]^{2+}$ concentration in the center (indicated by a decrease of the NMR signal). Thus, diffusion of $[Ni(H_2O)_6]^{2+}$ toward the core of the catalyst bodies took place. After 5 min, the center of the extrudates contained almost no $[Ni(H_2O)_6]^{2+}$, as deduced from the NMR signal intensity value, which was close to that of pure water (6×10^5 au). These signal intensity profiles indicated that $[Ni(H_2O)_6]^{2+}$ moved faster at pH 1 than at pH 6, due to the electrostatic repulsion between the positively charged alumina surface and $[Ni(H_2O)_6]^{2+}$. The inner ring that was formed when the catalyst body was impregnated with solution Ni*edta*6:1pH1 is not so easily visible in the 1D signal intensity profiles and is indicated with arrows in the figure. This is because for $[Ni(H_2O)_6]^{2+}$ concentrations above 0.5 M, large variations in the concentration give small variations of the NMR signal, as can be seen from the calibration curve depicted in the Supporting Information, Figure S1a.

An attempt to analyze the results was made under the assumption that the calibration curve (eq 1) constructed for the quantification of $[Ni(H_2O)_6]^{2+}$ transport is applicable in the presence of $[Ni(edtaH_x)]^{(2-x)-}$; i.e., when solutions Ni*edta*6:1pH1 and Ni*edta*6:1pH6 are used for impregnation. The resulting $[Ni(H_2O)_6]^{2+}$ concentration profiles obtained after 2 h and the corresponding T_2-weighted images of the impregnated extrudates are depicted in Figure 7. The apparent egg-white and egg-shell macro-distributions are clearly visualized in the 1D concentration profiles. The average $[Ni(H_2O)_6]^{2+}$ concentration in the core of the extrudates, regardless of the solution pH, was 0.52 M, which is in agreement with the concentration of $[Ni(H_2O)_6]^{2+}$ in the impregnation solution. However, the calculated concentrations of $[Ni(H_2O)_6]^{2+}$ in the positions where the NMR signal was the lowest were significantly higher (0.6−0.8 M, Figure 7). As a result, the average $[Ni(H_2O)_6]^{2+}$ concentrations over the entire cross section of the catalyst bodies impregnated with Ni*edta*6:1pH1 and Ni*edta*6:1pH6 solutions were calculated to be 0.56 and 0.60 M, respectively. Both values are higher than the 0.5 M $[Ni(H_2O)_6]^{2+}$ concentration of the impregnation solutions and outside the expected uncertainty. Therefore, the assumption about the applicability of the calibration curve (eq 1) for the quantification of the $[Ni(H_2O)_6]^{2+}$ concentration in the presence of other Ni^{2+} complexes may not be valid. This clearly indicates that $[Ni(edtaH_x)]^{(2-x)-}$ ions have an influence on the paramagnetic properties of the $[Ni(H_2O)_6]^{2+}$ ion, and consequently on the relaxation times of water protons when both complexes are present.

3.4. Dynamics of $[Ni(H_2O)_6]^{2+}$ and $[Ni(edtaH_x)]^{(2-x)-}$ within γ-Al_2O_3 Catalyst Bodies Based on UV−vis Microspectroscopy. Figure 8 shows the UV−vis profiles of the catalyst bodies after impregnation with solutions Ni*edta*6:1pH1 and Ni*edta*6:1pH6.

Parts a and b (left) of Figure 8 show clear changes in the UV−vis spectra measured from the edge (spectrum 6) to the core (spectrum 1) of the extrudates, after 5 min, regardless of the solution pH. Spectrum 1, in the core of the extrudate, suggests the only presence of NO_3^- ions ($n \rightarrow \pi^*$ charge-transfer transition at around 300 nm).[43] This observation corroborates the MRI data, which suggested the presence of pure water (Figure 6). The characteristic d−d absorption bands of $[Ni(H_2O)_6]^{2+}$ at 391, 654, and 730 nm were detected in spectra 2−4; however, they are slightly shifted to longer wavelengths (400, 659, and 738 nm).[43] The $[Ni(H_2O)_6]^{2+}$ d−d absorption band at 1100 nm was beyond the detection limit of the equipment, but its tail could also be visualized in spectra 2−4. The shift in the position of these bands suggested the exchange of water ligands by OH^- ligands or $Al-O^-$ from the alumina surface. The former ligands could come from the partial hydrolysis of this complex to form $[Ni(H_2O)_{6-x}(OH)_x]^{(2-x)+}$, due

(42) Bowers, A. R.; Huang, C. P. *J. Colloid Interface Sci.* **1986**, *110*, 575.

(43) Lever, A. B. P. *Inorganic Electronic Spectroscopy*; Elsevier Science B.V.: Amsterdam, 1987.

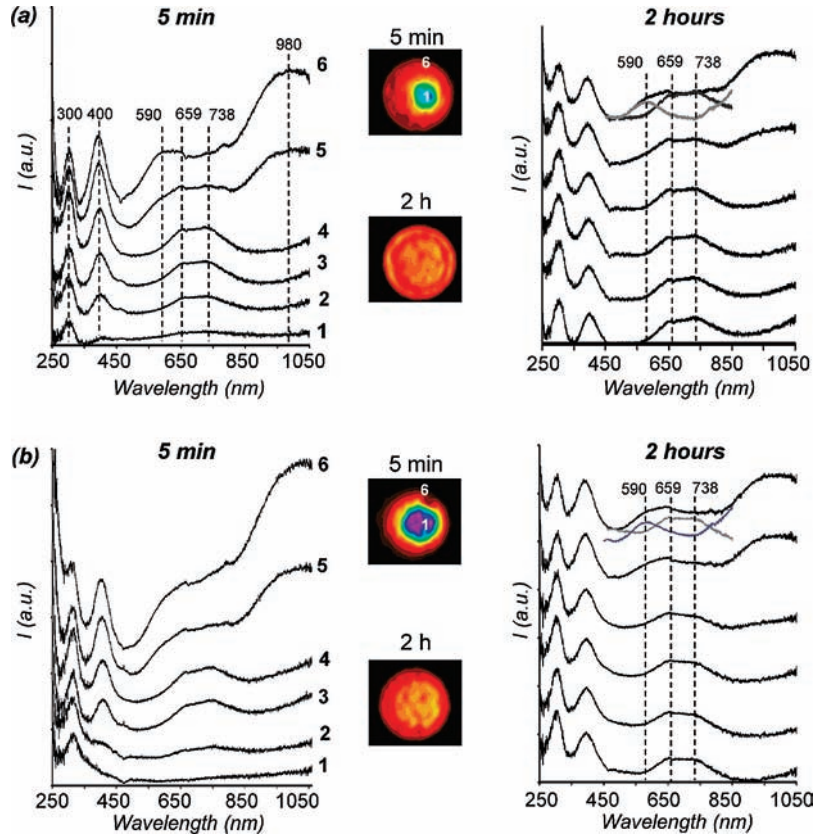

Figure 8. UV−vis profiles from the edge (6) to the center (1) of bisected catalyst bodies 5 min and 2 h after impregnation with solutions Ni*edta* 6:1pH1 (a) and Ni*edta* 6:1pH6 (b) and the corresponding T_2-weighted images.

to adsorption of the protons on alumina surface. The latter ligands would form $[Ni(H_2O)_{6-x}(O-Al)_x]^{(2-x)-}$ due to replacement of one or more of the water ligands with the surface oxygen atoms from γ-alumina.[6] The transport rates of Ni^{2+}, deduced from the Ni^{2+} absorption bands, in both impregnated bodies were in agreement with those observed with MRI. In particular, the d−d transition bands of $[Ni(H_2O)_6]^{2+}$ indicated that 5 min after impregnation this complex was closer to the center in the extrudate impregnated with solution Ni*edta* 6:1pH1. The spectra close to the edges (spectra 5 and 6), 5 min after impregnation, showed several bands. The 300-nm band indicative of NO_3^- was present, together with other three bands at around 400, 450−850, and 980 nm. These bands are assigned to the three d−d spin allowed transitions of six-coordinate octahedral or pseudo-octahedral Ni^{2+}, and their positions depend on the type of ligands.[43] The d−d transition bands for the complex $[Ni(edtaH_x)]^{(2-x)-}$ ($x = 0-2$) were observed at around 380, 590, and 980 nm with slight shifts in the positions and changes in the maximum absorption, depending on the protonation state of the complex.[44] The band at 400 nm is an indication of the presence of both $[Ni(H_2O)_6]^{2+}$ and $[Ni(edtaH_x)]^{(2-x)-}$. The shape of the band at 450−850 nm suggested the simultaneous presence of the complexes $[Ni(H_2O)_6]^{2+}$ (maximum absorption at around 659 and 738 nm) and $[Ni(edtaH_x)]^{(2-x)-}$ (maximum absorption at around 590 nm) regardless of the solution pH.[43,44] Moreover, the band at 980 nm corroborated the presence of $[Ni(edtaH_x)]^{(2-x)-}$ in the outer rim of the catalyst bodies.[44] The UV−vis spectra after impregnation of the same type of extrudates with the individual complexes $[Ni(H_2O)_6]^{2+}$ and $[Ni(edtaH_x)]^{(2-x)-}$ were also measured as a reference, these spectra are shown in Figure S9 of the Supporting Information.

Parts a and b (right) of Figure 8 show the UV−vis profiles 2 h after impregnation. After this time, $[Ni(H_2O)_6]^{2+}$ was the only species in the core of the extrudate, regardless of the solution pH; as indicated by the Ni d−d transition bands at 400, 659, and 738 nm. Thus, $[Ni(H_2O)_6]^{2+}$ diffused faster than $[Ni(edtaH_x)]^{(2-x)-}$. However, it was also present in the edges of the catalyst bodies, as deduced from the shape of the band at 450−850 in the edge. Deconvolution of the band at 450−850 nm in the edges of the catalyst body was done under the assumption that $[Ni(H_2O)_6]^{2+}$ was uniformly distributed, as explained in the Supporting Information. From the deconvolution of this band, the areas under the bands at 590 nm ($[Ni(edtaH_x)]^{(2-x)-}$) and at 659 + 738 nm ($[Ni(H_2O)_6]^{2+}$) could be calculated, their variation with position inside the extrudate is shown in the Supporting Information. Moreover, from these areas, the concentration profiles of both complexes and of the total Ni^{2+} concentration as a function of position in the catalyst body, 2 h after impregnation, could be estimated, see Figure 9.

The bands at 590 and 980 nm indicated that, regardless of the pH and time after impregnation, $[Ni(edtaH_x)]^{(2-x)-}$ species remain in the outer rim of the extrudates. Still, it is difficult to assign these bands to a particular $[Ni(edtaH_x)]^{(2-x)-}$ complex due to the strong similarity in the UV−vis spectra of the different $[Ni(edtaH_x)]^{(2-x)-}$ species ($x = 0-2$).[44] For reference purposes, these spectra are shown in the Supporting Information.

3.5. Combined MRI and UV−vis Microspectroscopy Study: Diffusion of Ni^{2+} Complexes and Their Interactions with the γ-Al_2O_3 Surface. A detailed analysis of the MRI and UV−vis microspectroscopic results lead to propose a model for diffusion

(44) Bhat, T. R.; Krishnamurthy, M. *J. Inorg. Nucl. Chem.* **1963**, *25*, 1147.

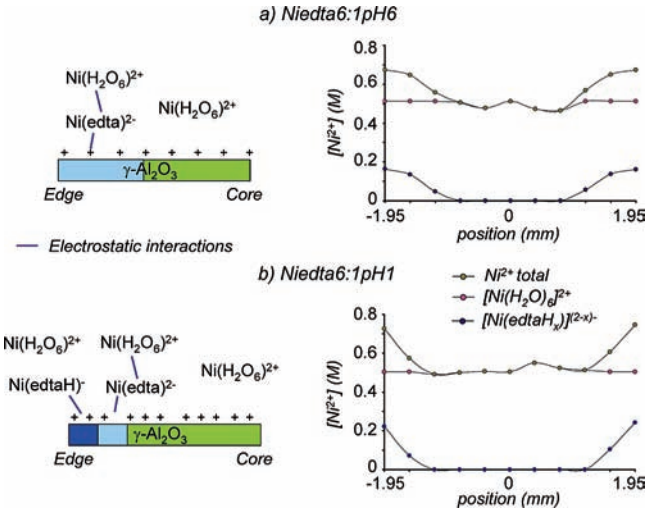

Figure 9. (Left) Adsorption mechanism of $[Ni(H_2O)_6]^{2+}$ and $[Ni(edtaH_x)]^{(2-x)-}$ on γ-Al_2O_3 surface 2 h after impregnation of extrudates with the solutions (a) Ni*edta*6:1pH6 and (b) Ni*edta*6:1pH1. (Right) Concentration distributions of these Ni^{2+} complexes and of the total Ni^{2+} concentration estimated from the UV−vis spectra as shown in Figure 8.

and adsorption/desorption on γ-Al_2O_3 surface of $[Ni(H_2O)_6]^{2+}$ and $[Ni(edtaH_x)]^{(2-x)-}$ as a function of pH, when these complexes are coimpregnated.

3.5.1. Solution Ni*edta*6:1pH6. Five minutes after impregnating the extrudate with the solution Ni*edta*6:1pH6, alumina becomes slightly positively charged since its pzc is 7.9.[45] For this reason, $[Ni(edta)]^{2-}$ interacts electrostatically with the γ-Al_2O_3 surface, while $[Ni(H_2O)_6]^{2+}$ does not. Therefore, the diffusion of $[Ni(edta)]^{2-}$ toward the core is slower than the transport of $[Ni(H_2O)_6]^{2+}$.

In addition, the protonation of the alumina surface brings about an increase of the solution pH inside the pores, especially in the edges of the extrudate. This increase is determined by the pzc of alumina and, therefore, cannot be higher than 7.9. The pH increase in the pores will not affect the molecular structure of the $[Ni(edta)]^{2-}$ complex since it is stable in the pH region of interest. However, $[Ni(H_2O)_6]^{2+}$, in the edges of the extrudate, can partially hydrolyze or even precipitate (in solution or at the surface). The formation of e.g. $[Ni(H_2O)_4(OH)_2]$ will cause a decrease of the solution pH which in turn stops the precipitation or hydrolysis and the remaining $[Ni(H_2O)_6]^{2+}$ can move forward.

After 2 h, UV−vis microspectroscopy indicates that $[Ni(H_2O)_6]^{2+}$ is present in the core and in the outer rim of the catalyst body, while $[Ni(edta)]^{2-}$ is only present in the outer rim. The $[Ni(H_2O)_6]^{2+}$ concentration in the core region, where this complex was unique, was evaluated from the MRI data as 0.52 M. Thus, its concentration in the edges should be approximately the same. The higher concentration values obtained in this region using eq 1 imply that this calibration is not valid when both $[Ni(edta)]^{2-}$ and $[Ni(H_2O)_6]^{2+}$ are present in solution. In other words, the local presence of both Ni^{2+} complexes in the edges of the extrudate leads to a stronger paramagnetic influence on the relaxation rate of water protons. This cannot be explained as a simple additive effect of the two paramagnetic complexes since, as demonstrated above, the effect of $[Ni(edta)]^{2-}$ is too small to be observed in the T_2-weighted images (Figure 4). Therefore, we have to conclude that the degree of paramagnetic influence of $[Ni(H_2O)_6]^{2+}$ on water protons changes in the presence of $[Ni(edta)]^{2-}$.

An adsorption mechanism, presented in Figure 9a, is suggested. When $[Ni(edta)]^{2-}$ is adsorbed on the positively charged alumina surface, the $[Ni(edta)]^{2-}$ negative charge is not totally compensated by the support's surface charge.[42,45,46] Therefore, the adsorption of $[Ni(edta)]^{2-}$ on alumina creates a negative layer or charge reversal of alumina surface, which enhances the electrostatic interaction between the surface layer and $[Ni(H_2O)_6]^{2+}$ and, thus, changes the paramagnetic influence of $[Ni(H_2O)_6]^{2+}$ on the relaxation of water protons. Hence, the actual overall Ni concentration profile 2 h after impregnation was egg-shell like, with a uniform 0.5 M $[Ni(H_2O)_6]^{2+}$ distribution and an egg-shell $[Ni(edta)]^{2-}$ profile (Figure 9a). Moreover, electrostatic interactions are taking place between the $[Ni(H_2O)_6]^{2+}$ and the negative surface layer created by adsorption of $[Ni(edta)]^{2-}$ on alumina surface in the edges of the extrudate. The concentration profiles of $[Ni(edta)]^{2-}$ and $[Ni(H_2O)_6]^{2+}$ shown in Figure 9a were estimated from UV−vis microspectroscopy, as explained in the Supporting Information.

3.5.2. Solution Ni*edta*6:1pH1. Five minutes after impregnating the extrudate with the solution Ni*edta*6:1pH1, a similar diffusion mechanism of $[Ni(edtaH_x)]^{(2-x)-}$ ($x = 1$ and 2) and $[Ni(H_2O)_6]^{2+}$ as at pH 6 takes place. At this pH value, γ-Al_2O_3 becomes even more positively charged. From the UV−vis profile and the MRI data after this time, it is possible to conclude that, again, $[Ni(edtaH)]^{-}$ adsorbs electrostatically at the edges of the extrudate. On the other hand, $[Ni(edtaH_2)]$ and $[Ni(H_2O)_6]^{2+}$ do not adsorb and move toward the core. $[Ni(H_2O)_6]^{2+}$, however, diffuses faster than $[Ni(edtaH_2)]$. The diffusion rate of $[Ni(H_2O)_6]^{2+}$ is faster at this pH than at pH 6. This occurs because the solution pH inside the pores of alumina, even though it increases, is more acidic than after impregnation of alumina with the solution at pH 6. Therefore, the hydrolysis of $[Ni(H_2O)_6]^{2+}$ occurs to a limited extent.

UV−vis microspectroscopic data 2 h after impregnation indicated the only presence of $[Ni(H_2O)_6]^{2+}$ in the core of the extrudate, and the presence of both $[Ni(H_2O)_6]^{2+}$ and $[Ni(edtaH_x)]^{(2-x)-}$ toward the edges (Figure 8a). From the concentration profile shown in Figure 7a, $[Ni(H_2O)_6]^{2+}$ concentration was calculated to be 0.52 M in the core of the catalyst body. Therefore, 0.52 M has to be also the concentration of $[Ni(H_2O)_6]^{2+}$ in the edges of the catalyst body. The T_2-weighted images demonstrated the presence of an inner ring with the lowest NMR signal of the cross-section of the catalyst body. The formation of this egg-white distribution at pH 1, compared to the egg-shell at pH 6, is linked to the presence of the two $[Ni(edtaH_x)]^{(2-x)-}$ ($x = 1, 2$) species instead of $[Ni(edta)]^{2-}$, present at pH 6. The different paramagnetic influence in the edges and in the inner ring (indicated by arrows in Figure 6 left) is most likely connected to the different interactions of $[Ni(edtaH)]^{-}$ and $[Ni(edtaH_2)]$ complexes with the alumina surface.

When an extrudate was impregnated with solution Ni*edta*6:1pH1, immediately after impregnation $[Ni(edtaH)]^{-}$ was adsorbed electrostatically at the edges of the extrudate on the positively charged alumina surface, and its charge could be totally compensated by the positive alumina hydroxyl groups.[42] In this position, no charge reversal of the alumina surface took

(45) Bourikas, K.; Kordulis, C.; Lycourgiotis, A. *Cat. Rev.−Sci. Eng.* **2006**, *48*, 363.

(46) Nowack, B.; Lutzenkirchen, J.; Behra, P.; Sigg, L. *Environ. Sci. Technol.* **1996**, *30*, 2397.

place, and $[Ni(H_2O)_6]^{2+}$ that was present did not interact electrostatically with this species. Consequently, the paramagnetic influence of $[Ni(H_2O)_6]^{2+}$ on water protons was not enhanced. At the same time, the complex [Ni(*edta*H_2)] moved deeper in the extrudate since its neutral charge prevents it from interacting electrostatically with the alumina surface. However, the solution pH increases during its transport toward the core. Therefore, this complex underwent acid−base reactions with hydroxyls on alumina surface. [Ni(*edta*H_2)] could deprotonate, while moving toward the core, and formed [Ni(*edta*H)]$^-$ and [Ni(*edta*)]$^{2-}$, with the latter being stable at pH above 2.5. Within an inner ring, the electrostatic adsorption of [Ni(*edta*)]$^{2-}$ on the alumina surface could result in charge reversal of the surface and promote the electrostatic adsorption of $[Ni(H_2O)_6]^{2+}$ on [Ni(*edta*)]$^{2-}$, as explained previously, and enhanced the relaxation rate of water protons. The higher relaxation rate of water protons in the inner ring resulted in the apparent egg-white concentration profile. The interactions between the Ni^{2+} complexes due to charge reversal are depicted schematically in Figure 9b. However, the actual Ni concentration profile estimated from UV−vis and MRI data was egg-shell with a 0.5 M uniform distribution of $[Ni(H_2O)_6]^{2+}$ and an egg-shell like distribution of Ni-*edta* species, similar to that obtained after impregnation with the solution Ni*edta*6:1pH6, see Figure 9b (right).

To summarize, the quantitative $[Ni(H_2O)_6]^{2+}$ concentration profiles calculated from the NMR images in the presence of $[Ni(edtaH_x)]^{(2-x)-}$ were only valid in the core of the catalyst bodies; i.e., in the region where this complex was unique. The overall Ni macro-distribution was egg-shell, regardless of the solution pH. In the outer rim of the catalyst body, the paramagnetic influence of $[Ni(H_2O)_6]^{2+}$ on the relaxation of water protons was enhanced due to the presence of [Ni(*edta*)]$^{2-}$. The different signal intensity profiles obtained, depending on the solution pH, suggested that the relaxation rate of water protons depends on the type and strength of the interactions of the Ni^{2+} complexes with each other and with the support surface. In other words, the electrostatic interactions between [Ni(*edta*)]$^{2-}$ and $[Ni(H_2O)_6]^{2+}$ increase the relaxation rate of water protons. On the contrary, the presence of [Ni(*edta*H)]$^-$ does not significantly change the paramagnetic influence of $[Ni(H_2O)_6]^{2+}$ on the water protons since no electrostatic interactions are present once [Ni(*edta*H)]$^-$ is adsorbed on the alumina surface.

4. Conclusions

MRI shows potential as a general method to monitor transport processes in a quantitative manner when millimeter-sized catalyst bodies are impregnated with single paramagnetic components. $[Ni(H_2O)_6]^{2+}$ was chosen as a model to apply this method, and quantitative data about the spatial distribution of the complex and its transport upon impregnation were obtained. This technique has also been demonstrated to be a valuable tool to monitor the dynamics of shielded paramagnetic metal ion complexes, such as [Ni(*edta*)]$^{2-}$, by implementing T_1 instead of T_2 contrast in the MRI experiment. MRI was also able to visualize the transport of Ni^{2+} when two different species, such as $[Ni(H_2O)_6]^{2+}$ and $[Ni(edtaH_x)]^{(2-x)-}$, were present inside the catalyst body. Moreover, UV−vis microspectroscopy enabled the perfect location of $[Ni(H_2O)_6]^{2+}$ and $[Ni(edtaH_x)]^{(2-x)-}$. After 2 h, the former was present along the cross section of the extrudate, while the latter remained in the outer rim of the catalyst body. This information enabled the use MRI in a quantitative manner for determining the $[Ni(H_2O)_6]^{2+}$ concentration distribution in the presence of $[Ni(edtaH_x)]^{(2-x)-}$. Additionally, MRI provided indirect information on the interactions of different Ni^{2+} complexes with each other, and with the surface of the support. These interactions, which already occur in the first stage of catalyst preparation, are directly responsible for the final metal-concentration distributions in the extrudate and for its final metal phase(s) and dispersion. The combination of the two techniques facilitated the understanding of the transport and adsorption of the different species on the surface of the support. More specifically, the use of *edta* in a low *edta*:Ni^{2+} molar ratio suggested the formation of Ni^{2+} egg-shell distributions, when acidic pH was used, with the *edta* ligand acting as a linker between Ni^{2+} and the alumina surface. These profiles, which are not easy to achieve in the preparation of Ni catalyst bodies, are interesting profiles in chemical reactions with diffusional restrictions.

Acknowledgment. We acknowledge financial support by ACTS-ASPECT. A.A.L. and I.V.K. thank the Russian Academy of Sciences (Grant 5.1.1), the Siberian Branch of the Russian Academy of Sciences (Integration Grant 67), the Russian Foundation for Basic Research (Grants 08-03-00661, 08-03-91102, and 07-03-12147), and the program of support of leading scientific schools (Grant NSh-3604.2008.3). A.A.L. acknowledges the Council on Grants of the President of the Russian Federation (MK-5135.2007.3).

Supporting Information Available: Details on the determination of the calibration curve which relates $[Ni(H_2O)_6]^{2+}$ concentration and NMR signal intensity, and on the UV−vis (micro)spectroscopy of Ni-*edta* solutions and of the impregnated catalyst bodies. This material is available free of charge via the Internet at http://pubs.acs.org.

JA900346K